

Nanoscale

Accepted Manuscript

This article can be cited before page numbers have been issued, to do this please use: H. Barhum, D. S. Kolchanov, M. Attrash, R. Unis, J. Alnis, T. Salgals, I. Yehia and P. Ginzburg, *Nanoscale*, 2023, DOI: 10.1039/D3NR02744A.



This is an Accepted Manuscript, which has been through the Royal Society of Chemistry peer review process and has been accepted for publication.

Accepted Manuscripts are published online shortly after acceptance, before technical editing, formatting and proof reading. Using this free service, authors can make their results available to the community, in citable form, before we publish the edited article. We will replace this Accepted Manuscript with the edited and formatted Advance Article as soon as it is available.

You can find more information about Accepted Manuscripts in the [Information for Authors](#).

Please note that technical editing may introduce minor changes to the text and/or graphics, which may alter content. The journal's standard [Terms & Conditions](#) and the [Ethical guidelines](#) still apply. In no event shall the Royal Society of Chemistry be held responsible for any errors or omissions in this Accepted Manuscript or any consequences arising from the use of any information it contains.

ARTICLE

Received 00th January 20xx,

Accepted 00th January 20xx

DOI: 10.1039/x0xx00000x

Thin-film Conformal Fluorescent SU8-PhenylenediamineHani Barhum^{*abc}, Dennis Kolchanov^{bc}, Mohammad Attrash^d, Razan Unis^{ae}, Janis Alnis^f, Toms Salgals^g, Ibrahim Yehia^a, and Pavel Ginzburg^{bc}

SU8 polymer is a negative photoresist widely used to produce high-quality coatings, with controllable thicknesses ranging from nanometers to millimeters, depending on fabrication protocols. Apart from conventional use cases in microelectronics and fluidics, SU8 is quite an attractive platform in nanophotonics. This material, being straightforwardly processed with ultraviolet lithography, is transparent to wavelengths longer than 500nm. However, introducing fluorescent agents within the SU8 matrix remains a challenge owing to its high hydrophobicity. Here we develop a process, where colorful quantum dots co-participate in the polymerization process by epoxide amination and become a part of a new fluorescent material – SU8-Phenylenediamine. Through comprehensive characterization methods, including XPS and ¹H-NMR analyses, we demonstrate that m-PD covalently binds to SU8 epoxy sites with its molecular amine., virtually forming a new material and not just a mixture between two compounds. After characterizing the new strongly fluorescent platform, thin 300nm films were created on several surfaces, including a conformal coverage of a nanofluidic capillary. This new process opens opportunities to incorporate various functional molecules into optoelectronic devices without a penalty of multistep deposition and surface functionalization.

^a Triangle Regional Research and Development Center, Kfar Qara' 3007500, Israel.^b Department of Electrical Engineering, Tel Aviv University, Ramat Aviv, Tel Aviv 69978, Israel.^c Light-Matter Interaction Centre, Tel Aviv University, Tel Aviv, 69978, Israel.^d Andrew and Erna Viterbi Department of Electrical Engineering, Technion, Haifa.^e Department of Environmental Studies, Porter School of Environment and Earth Sciences, Tel Aviv University, Tel Aviv, Israel.^f Institute of Atomic Physics and Spectroscopy, University of Latvia, Jelgavas Street 3, 1004 Riga, Latvia.^g Institute of Telecommunications, Riga Technical University, 12 Azenes Street, 1048 Riga, Latvia.

* Corresponding author.

Electronic Supplementary Information (ESI) available: [details of any supplementary information available should be included here]. See DOI: 10.1039/x0xx00000x



ARTICLE

Introduction

SU8 epoxy-based photoresist has gained significant attention since it was first introduced in 1995¹. Since epoxy groups are crosslinked by being exposed to ultraviolet (UV) light (typically, 365-405nm) and form a stable solid structure, the polymer belongs to the family of negative photoresists^{2,3}. After revealing numerous advantages of SU8, it became a technological platform across many disciplines, including microfluidics⁴⁻⁷, micromechanics⁸, biomedicine⁹, optoelectronics^{10,11}, and many others¹²⁻¹⁵.

Superior mechanical and thermal stability along with great adhesion to a vast majority of commonly used surfaces (e.g., glasses⁷, metals¹⁶, semiconductors¹⁷, and many others¹⁸) make SU8 a platform of choice in cases when facile low-cost fabrication of microstructures is required^{18,19}. For example, structures with sharp edges and high aspect ratios, approaching 1:20, 1:40, and even higher can be fabricated with photolithographic methods²⁰. Furthermore, spin-coating protocols with accurately controlled parameters allow fabricating film with thicknesses ranging between sub-micron up to millimeters¹⁵.

Apart from its mechanical properties, SU8 is also an optically transparent material. Having a strong absorption in the UV range owing to benzene rings, the material is transparent for wavelengths longer than ~500nm^{21,22}. Due to its optical and mechanical properties, SU8 is employed for fabricating micro-fluidic channels, routinely used in various biological studies, e.g., for cell culturing²³. Three-dimensional SU8-based devices allow mimicking microenvironments experienced by cells in a complex tissue^{9,24}. Incredible advances in the growth and differentiation of neural and muscle cells²⁵ encompass significant microfluidic components, where engineered thin-layer polymers play a role³¹. Microfluidic channels were developed to guide axonal development towards the muscle cells, paving the way for a deeper understanding of the pathology of amyotrophic lateral sclerosis (ALS)²⁶. Along with biological studies, many photonic applications have been explored. Waveguiding structures for sensing applications and integration within on-chip photonic circuits^{11,12}, Mach-Zehnder SU8-based interferometers^{27,28}, and on-chip microresonator-based biosensors with near-edge resonance^{10,29} have been demonstrated to name just a few. Consequently, functionalized photonic and microfluidic SU8 technologies have emerged at the forefront of this rapidly evolving field, offering promising new possibilities and applications.

To grant SU8 with additional optical properties, a structural functionalization with nanoparticles was demonstrated, introducing a range of plasmonic phenomena into light-matter interaction scenarios³⁰. A direct linkage between molecular species and SU8 is quite appealing, and it is mainly done with the APTMS-Glut chemical binding to the surface enabling covalent attachment of desired molecules. The SU8's high hydrophobicity limits the interaction to the same kind of materials³¹. The low interaction forces with different materials along with the high chemical potential from the radical ester make its specific and liable bonding a nontrivial target. Since SU8 is widely used in biomedical studies, its functionalization is better to be performed with biocompatible fluorescent materials³²⁻³⁴. The biocompatibility of fluorescent agents is a significant area of its own, demanding the development of new platforms. Our focus is on phenylenediamine carbon dots, as we recently mastered their facile fabrication and sensing applications³⁵. Specifically, a 90% reaction yield of carbon dots with a 70% quantum yield was demonstrated. As a result, matching those emitters with low-cost SU8 polymer might have future technological benefits.

Here, we take advantage of the epoxy group in SU8 polymer to spontaneously bind amine groups of phenylenediamine carbon dots. The covalent bonding of the molecules is integrated into the organic polymer skeleton, virtually forming a new material. This process turns the structure to provide an inherently efficient fluorescence, which motivates the use of this new polymer in nanophotonics applications. To



ARTICLE

demonstrate the concept, we fabricated a series of devices by spin-coating thin films on flat coverslips and inner surfaces of micron-scale capillaries, which can be further designed for fluidic applications.

The manuscript is organized as follows: fabrication methods are presented first and then followed by an analysis and discussion on possible chemical reactions, responsible for the material formation. Then optical properties are presented of the bulk material with different aniline isomers. The characterization results are used for the structure analysis with molecular dynamic methods to predict the chemical composition and band gap. Fabrication of thin films and surface conjugation is discussed before the Conclusion.

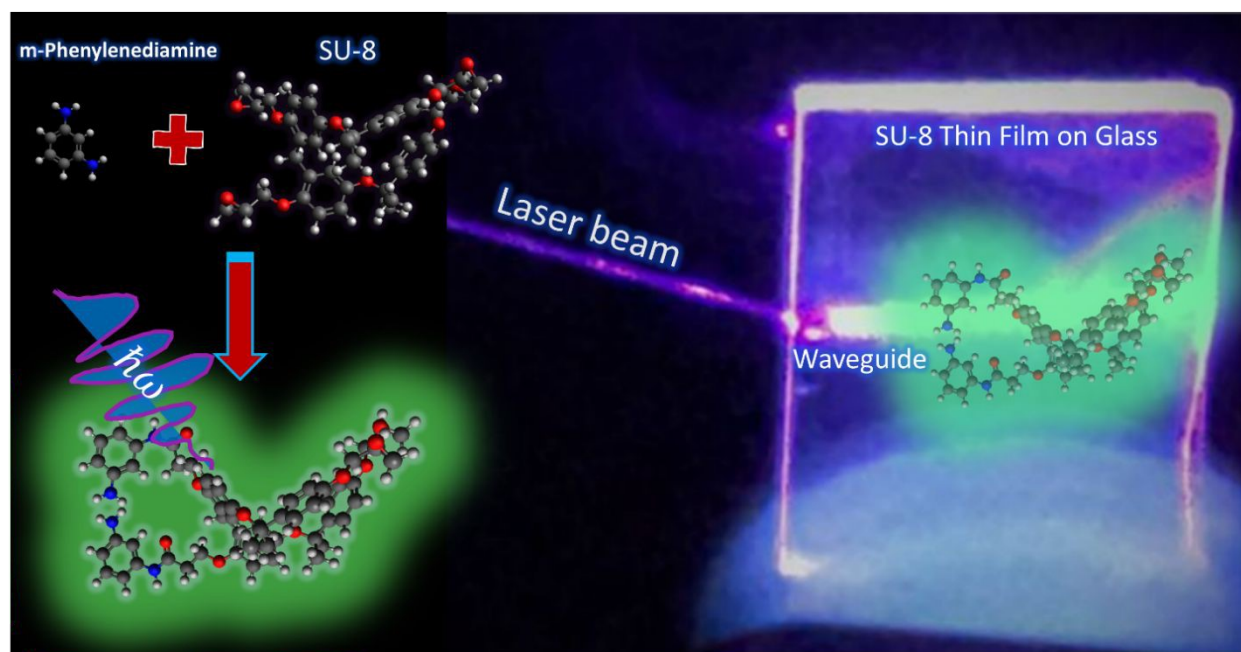


Figure 1: Graphical illustrations and a practical application of the SU8 polymer before and after conjugation with m-phenylenediamine (m-PD). The upper left panel represents the dimeric form of the SU8 polymer prior to the conjugation process with m-PD. The lower left panel shows the resulting structure post-conjugation, depicting the modifications imparted to the SU8 polymer by the m-PD. The right panel showcases a possible optoelectronic application: a glass slide with the polymer deposited onto its surface, and a waveguide fabricated within the polymer using a laser.



ARTICLE

Methods

Materials

The materials were purchased from: photoresist SU8-2000.5, 3005, 3050 -, Poly (ethylene glycol) methyl ether acrylate (PEGMEA) and SU8 developer Bachem (UK) Ltd, Meta-phenylenediamine (m-PD), ortho-phenylenediamine (o-PD), para-phenylenediamine (p-PD), Hydrochloric Acid (HCl), from Merck Ltd and 18M Ω water.

SU8 conjugation to phenylenediamine

First, the solution of the desired phenylenediamine isomer (para, ortho, meta, staying for a location on the amine group on the benzene ring³⁵) is dissolved by sonication in SU8 developer or in PEGMEA. The saturated solution is added in different amounts, to a 5 mL polymer solution and mixed on a shaker. Visual inspection by observing the color of the product is done once the light yellow SU8 turned into dark green solution (after 24 hours) spectral changes occurred during mixing until stabilized the tracking was not quantified into kinetic data. HCl addition to the reaction mixture is done from a concentrated solution. All the concentrations are detailed in the results section, where their impact on the resulting product is studied.

Film deposition and Surface functionalization

Thin films were deposited on different substrates pre-cleaned with Acetone and then rinsed with ethanol. After that, dried substrates are placed in a piranha solution until no bubbling appeared. Then samples were washed with DIW followed by EtOH and dried on a hot plate. M-PD saturated solution in Hexane was prepared by vigorous mixing and sonication.

Functionalization was performed by sequentially immersing freshly prepared, unpolymerized SU-8 film on a previously cleaned glass substrate with Piranha solution, and then dipped in m-PD saturated solution in Hexane for 5 minutes, followed by washing in pure Hexane for 1 min, and crosslinking the sample on a plate heated to 105 °C for 10 min.

Optical properties of conjugated SU8

Optical absorbance and fluorescence data were gathered using photoluminescence excitation (PLE) spectroscopy, carried out with a Synergy H1 plate reader. Absorbance spectra were obtained using a Macys1100 spectrophotometer, which featured a tungsten lamp source and a silicon photodiode detector. The instrument's spectral band was set at 2 nm, maintaining an accuracy of 1 nm. Prior to the tests, samples were diluted with deionized water. Fluorescent lifetime measurements were conducted using a PicoQuant system, employing a Taiko picosecond diode as a 375 nm excitation source. Lastly, confocal images were captured using the Leica 8 system.

ATR-Fourier Transform Infrared Spectroscopy (FTIR), Proton Nuclear Magnetic Resonance ¹H-NMR

The analysis was carried out using a Nicolet iS10 FTIR Spectrometer equipped with a KBr/Ge beam splitter, optimized for the mid-infrared range, and a fast recovery deuterated triglycine sulfate (DTGS) detector. In this study, solid samples were analyzed in compliance with ASTM



ARTICLE

E1421 standards using the aforementioned spectrometer. The resultant FTIR data played an instrumental role in deciphering the molecular interactions between m-PD and SU8.

For the ¹H-NMR analysis, dried and purified SU8-MPD powder was dissolved in chloroform and then introduced into a Bruker Ascend 500 High Resolution NMR machine operating at a magnetic field of 500MHz (11.7 Tesla). Spectra were obtained from both the SU8 and SU8-MPD samples after 48 hours of mixing.

Atomic force and electron scanning microscopy.

Film surface and thickness cross-section of polymer film characterizations were performed in an environmental electron scanning microscope (ESEM). The surface roughness is further characterized in JPLEC atomic force microscope (AFM).

Theoretical calculations

Theoretical calculations were performed by CP2K code³⁶, which uses a Gaussian basis set complemented by an auxiliary plane-wave basis. Structures were drawn by the VESTA code³⁷. We used a triple- ζ polarization quality Gaussian basis set (TZVP-MOLOPT-GTH)³⁸ and a 300 Ry plane-wave cutoff. The Broyden performed geometry optimization of the sample sletcher–Goldfarb–Shanno (BFGS) routine using the Gaussian plane-wave (GPW) method with the combined density functional of B88 (exchange functional) and LYP³⁹, where all atoms were relaxed until the residual force was smaller than 0.05 eV/Å. We applied a structural minimization algorithm using a non-periodic model in the Γ -point approximation. The electronic structure was investigated using the hybrid functional B3LYP⁴⁰.

Results and discussion

Functionalizing SU8 polymers with fluorescent molecules presents distinct challenges. Typically, this process involves chemical binding at specific sites, facilitated by crosslinking molecules. However, changes in the dye's electronic structure during this process can potentially degrade their fluorescence. Notably, aggregate dye molecules may undergo concentration quenching effects, further impacting their fluorescence, e.g.,⁴¹. Therefore, refining the chemistry to achieve fluorescent polymers with high quantum yield becomes imperative.

Optical properties of SU8-Phenylenediamine

Our exploration centers around the synthesis and optical properties of SU-8 polymers conjugated with phenylenediamine isomers, emphasizing the meta isomer (m-PD). Preliminary investigations distinguished m-PD for its superior fluorescent properties, exhibiting defined excitation and emission peaks and an enhanced emission intensity under increasing HCl concentrations. The Supplementary Information discusses the exhaustive comparative analyses involving o-PD and p-PD in detail (see Figure S1).

The SU8 polymers display distinct absorbance properties based on their viscosity. For example, SU8-2000.5 reveals an increased absorbance around 410 nm, with a pronounced peak observed at 0.65 M HCl (Figure 2(a)). SU8-3005 and SU8-3050 exhibit similar absorption characteristics



ARTICLE

(Figures 2 b, c). A deeper insight into the corresponding PLE spectra is shown in (Figures 2 d-i) and the variations in emission intensities can be referred to in the Supplementary Information.

To provide a comprehensive understanding of the optical modifications that emerge in the conjugated polymers, the characteristic peak values have been plotted against proton concentration in Figure S2. The identified trends imply that both the polymer's viscosity and the reaction medium's acidity exert substantial influence on the conjugation efficiency and the enhancement of fluorescence properties.

It is hypothesized that polymers with higher viscosity hinder the mobility of phenylenediamine molecules, consequently affecting the rate of conjugation and influencing the resulting absorbance and emission properties. Additionally, the acidity of the reaction medium can significantly impact the conjugation process. In this context, understanding the complex interactions between polymer viscosity, the acidity of the reaction medium, and the conjugation efficiency becomes crucial for optimizing the optical properties of these innovative conjugated materials. The collected data indicates that the absorbance of the conjugated SU8-2000.5 drops with the inclusion of HCl, while SU8-3005 and SU8-3050 seem to reach saturation at 0.65 M of acid. This observation can likely be attributed to the medium's viscosity, which facilitates more substantial conjugation and intricate pathways, as suggested, and will be further elaborated in our hypothesized model in section 3.2. This insight also implies that comprehensive conjugation of m-PD molecules occurs at the polymer chains, leading to enhanced absorbance or extinction, as represented in Figure S2(a).



ARTICLE

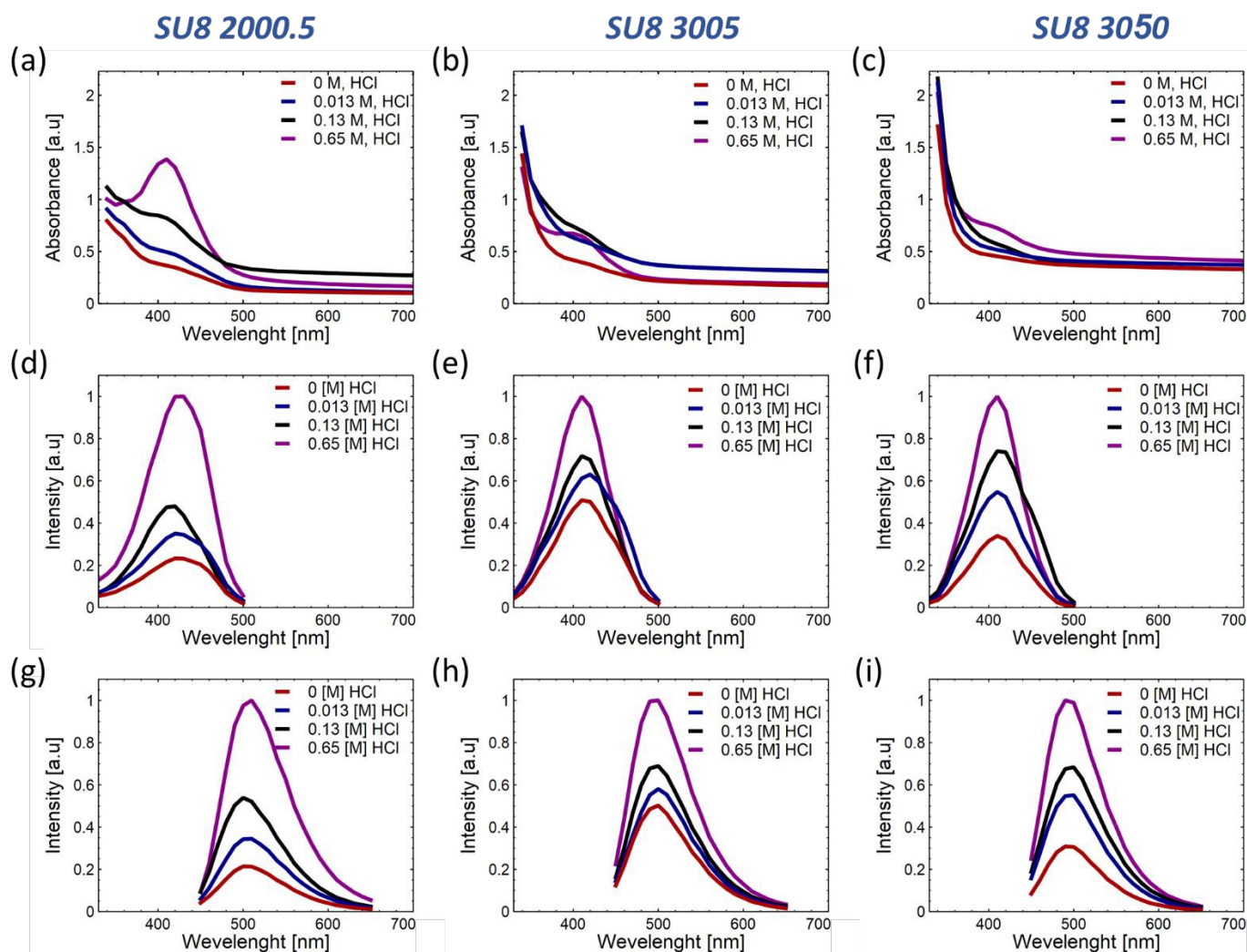
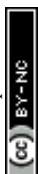


Figure 2: Optical properties of SU8 polymers with varying viscosities (SU8-2000.5, SU-8-3005, and SU8-3050) conjugated with *m*-PD molecules and the influence of different hydrochloric acid additions to the reaction medium. The first column represents SU8-2000.5, the second - SU8-3005, and the third - SU8-3050. (a, b, c) Absorbance spectra at 330 nm to 700 nm illustrate the impact of polymer viscosity. (d, e, f) PLE spectra (normalized) of the 530 nm emission peak, measured between 330 nm and 500 nm, highlighting the excitation-dependent behavior of the conjugates with varying viscosities. (g, h, i) Emission spectra (normalized) at 450 nm and 650 nm range with an at 420 nm.

Interestingly, the SU8-2000.5 polymer displays a maximum PLE intensity at 0.13 M HCl, while the other polymers present a gradual increase that moderates at higher concentrations, as illustrated in Figure S2(b). The relatively lower viscosity and polymer concentration of SU8-2000.5 refers to the formation of more conjugation and bonds between the *m*-PD and polymer, as well as among polymer chains. However, this



ARTICLE

process could also create additional bonds that do not contribute to fluorescence and might even interfere with some fluorescent sites. As observed in Figure S2 (b, c), the rise in fluorescence intensity for SU8-3005 and SU8-3050, alongside the decrease in intensity for SU8-2000.5, which allows assuming that the bonds formed in the initial stages of the reaction contribute more significantly to the formation of fluorescent species, while the later-formed bonds do not have the same impact. Furthermore, when the concentration of acid outstrips the availability of epoxy sites, the rate of formation of non-contributing bonds increases, thereby potentially disrupting the fluorescent conjugated spots. After observing the macroscopic optical properties of the SU8-m-PD, the molecular mechanisms of the material formation will be explored.

Molecular conjugations to phenylenediamine

The synthesis of m-PD conjugated with SU8 epoxy begins with the reaction between the amine group of m-PD and epoxy groups of SU8, resulting in the formation of secondary amines and the opening of epoxy rings. The reaction continues, leading predominantly to the formation of tertiary amines. This forms our starting point of investigation. It's important to acknowledge that this model, while informed by DFT modeling and an array of collected experimental data, is postulated based on current understanding and findings. It's built on extensive literature about amine to epoxy reactions and supported by our DFT calculations, but it's still, inherently, a proposition open for further investigation and refinement. Apart from fluorescent studies, FTIR spectra were required to shed light on the complex reaction. The spectrum evolution by adding m-PD at different concentrations offers insights into the chemical transformation occurring during this synthesis as shown in Figure 3.

In Figure 3 (a), the spectrum of pure SU8 displayed peaks representative of different bonds within the polymer. The aromatic ring-related C-C stretching⁴²⁻⁴⁷ vibrations were revealed through peaks at 559.60 cm⁻¹, 658.42 cm⁻¹, and 754.18 cm⁻¹. The peak at 910.23 cm⁻¹ indicated the presence of epoxy groups due to the characteristic C-O stretching vibrations. With the addition of m-PD to SU8, the spectra showed noticeable changes as seen in Figure 3 (b-c). A new peak emerged at 1055.43 cm⁻¹, which might indicate C-N stretching vibrations, potentially confirming the formation of secondary amine bonds.

Further addition of m-PD resulted in a continued decrease in intensities of epoxy-associated peaks, as shown in Figure 3 (d). Concurrently, there was an increase in the intensity of peaks around 3680.24 cm⁻¹ and 3705.38 cm⁻¹, hinting at the conversion of epoxy groups to free hydroxyl groups. It is also worth noting that secondary amine formation might be debatable, as FTIR peaks might shift and smear.



ARTICLE

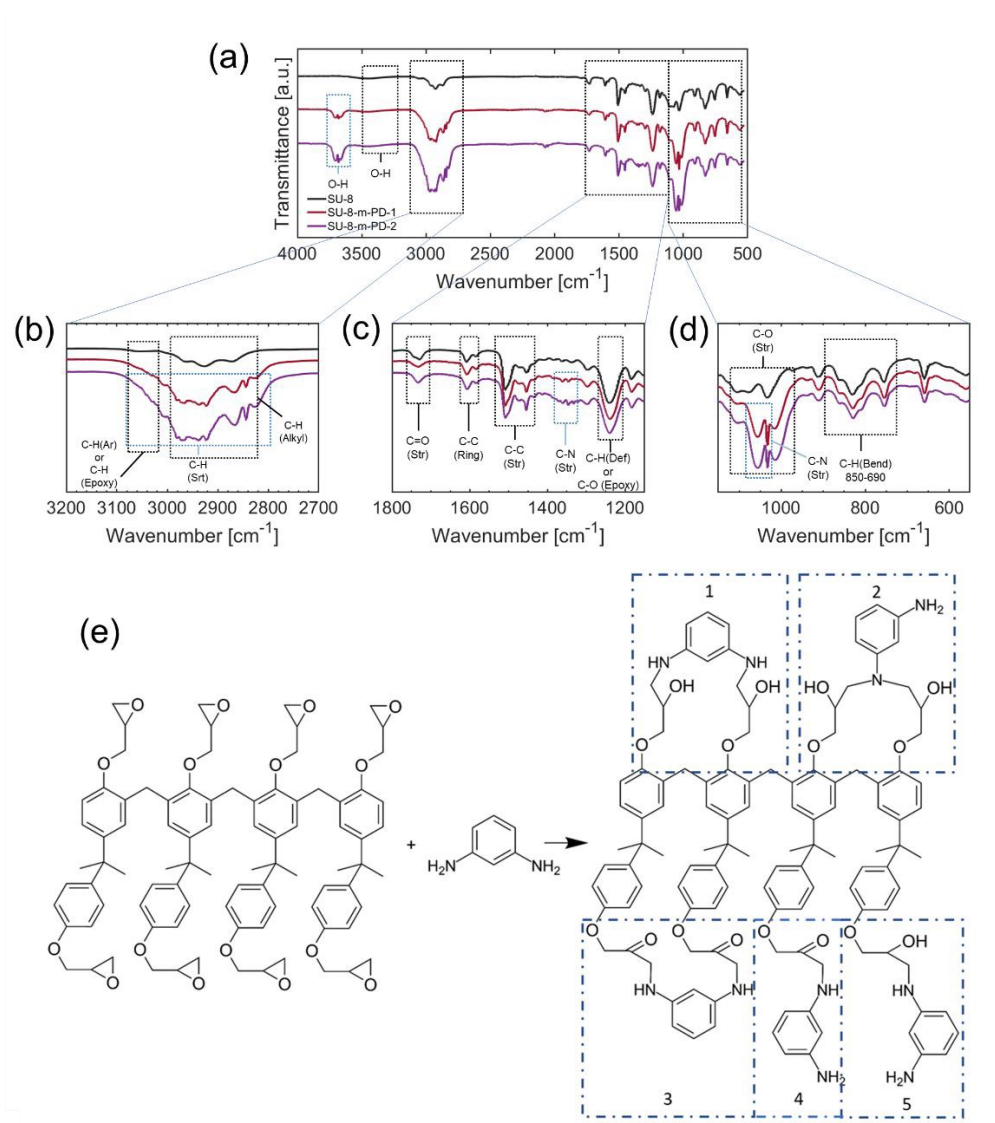


Figure 3: (a) Full-range ATR Fourier-transform infrared spectroscopy (FTIR) spectra of the conjugation process between meta-phenylenediamine (m-PD) and SU8, indicating the characteristic peaks corresponding to the functional groups involved. This spectrum provides an overview of the complex interactions that transpire during the conjugation process. (b) Detailed FTIR spectra in the 2800-3100 cm⁻¹ region, highlighting the specific vibrations attributed to various functional groups. (c) FTIR spectra in the 1150-1800 cm⁻¹ region, further delineating the presence of different functional group vibrations, including the potential formation of secondary amine and amide bonds. (d) FTIR spectra in the 1150-550 cm⁻¹ region, emphasizing the broad range of potential functional group interactions. The distinct peaks in this region are instrumental in deducing the nature of the interactions. (e) Several structures among the proposed configurations, while other options are analyzed further and hypothesized as less probable, and except model2 the others are first stage toward tertiary amination.



ARTICLE

Looking at Figure 3 (e), the primary product of the reaction appears to be the formation of tertiary aromatic amines. Interestingly, there was a lack of N-H stretching peaks in the range of 3400-3200 cm^{-1} , leading us to believe that all m-PD is used up during the reaction, without the significant formation of primary or secondary amines.

There was, however, debate around the existence of primary and secondary amines. Some suggested that terminal groups could remain as primary or secondary amines, despite the absence of clear evidence in the FTIR data. Also, the possibility of hidden peaks under the dominant signals around 3000 and 3600 cm^{-1} was raised. A different perspective on the formation of N-N or N-O bonds was also presented. Although the FTIR spectra didn't show clear evidence, the theoretical feasibility was suggested through DFT calculations.

Building upon the data presented in Figure 3 from the FTIR spectrum, we turn to Figure 4 $^1\text{H-NMR}$ spectrum to further probe the interaction between m-PD and SU8 epoxy. In Figure 4 (a), the overall $^1\text{H-NMR}$ spectrum provides a foundational reference, setting the stage for more detailed analysis. Figure 4 (b), focusing on the region from 0 to 2.25 ppm, predominantly captures the resonances of aliphatic protons inherent to the SU8 structure. This suggests that the core structure of SU8 remains unaffected mainly after the conjugation process. Transitioning to Figure 4 (c), which encompasses the 2.25-4.5 ppm region, we observe potential indications of the secondary or tertiary amine structures. The integration values within this region align with our previous observations from the FTIR study, hinting at the formation of secondary amines and possibly the evolution to tertiary amines. Lastly, in Figure 4 (d), ranging from 6.5 to 8 ppm, the aromatic proton signals come to the forefront. A notable shift in integration values from the sole SU8 to the m-PD conjugated SU8 provides indirect evidence of m-PD's aromatic protons finding their place within the new structural framework. This shift reaffirms that m-PD has successfully interacted with the SU8 epoxy.

The data from Figure 4 $^1\text{H-NMR}$ spectrum lends further credence to our proposed reaction mechanism and complements our FTIR findings. The subtle yet discernible changes across different regions of the spectrum paint a coherent picture of the chemical transformation underway.



ARTICLE

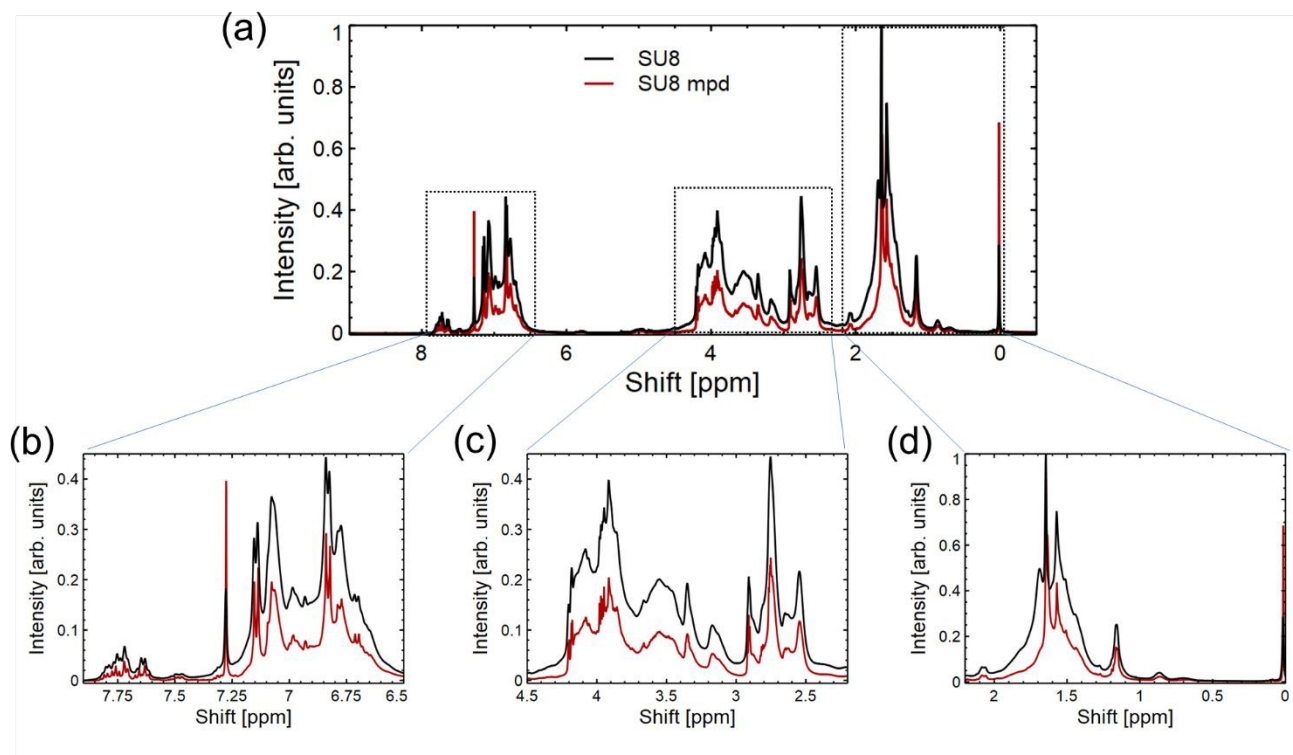


Figure 4: $^1\text{H-NMR}$ analysis of the SU8-mPD conjugate. (a) Provides a full view of the entire spectrum. Region-specific magnifications further elucidate the interactions: (b) Emphasizing the 6.5-8 ppm range, which is dominated by aromatic proton resonances, indicative of the SU8 and m-PD aromatic structures. (c) The 2.25-4.5 ppm region, highlighting potential transitional groups and intermediates; and (d) Focusing on the 0-2.25 ppm range, predominantly showcasing aliphatic proton environments.

X-ray photoelectron spectroscopy (XPS) provides detailed insights into the surface atomic composition of materials. Analyzing Figure S3(a-c) for pure SU8 and Figure S3(d-f) for SU8-mPD, distinct elemental variations emerge that substantiate the integration of m-PD into the SU8 matrix. Table S1 elucidates the atomic percentages for the SU8 sample, highlighting prominent peaks for carbon (C 1s, 71.93%) and oxygen (O 1s, 22.44%). With the conjugation to m-PD, as represented in Table S2, the carbon content slightly elevates to 73.01%, while the oxygen experiences a marginal decrement to 21.90%. However, the defining evidence is the emergence of the N 1s peak at 1.22%, absent in the pure SU8 sample.

Mathematically, let the content of m-PD in the SU8-mPD composite be represented by p . Based on the atomic ratios derived from the XPS data and the structure of m-PD, we estimate:

$$p \approx \frac{1.22\%(N1s)}{6(Catoms) + 2(Natoms)} \text{ eq.1}$$

From this equation, we deduce that the m-PD content in the SU8-mPD composite ranges between 4.88% to 9.95%. This gives us a m-PD:SU8 monomer ratio ranging from 1:19.5 to 1:10.05. These XPS findings, evident from Tables S1 and S2, consistently align with the transformations observed in Figure 3 from the FTIR analysis and the variances in aromatic and aliphatic regions seen in Figure 4 from the $^1\text{H-NMR}$ spectrum.



ARTICLE

Collectively, these results form a cohesive narrative, reinforcing the hypothesis of the successful conjugation of m-PD to the SU8 structure. Moreover, the XPS data extends our understanding by offering quantitative insight into this conjugation, strengthening the foundation for further explorations into modified SU8 systems.

DFT calculations

The m-PD and SU8 reaction is hypothesized relying on DFT calculations and available experimental data. A range of plausible molecular configurations will be proposed next, offering a unique perspective on how m-PD and SU8 interact, illustrated in Figure 5 (a-d). Starting with Figure 5 (a), a tertiary amine formation is shown, which involves an m-PD molecule and an SU8 monomer. Here, the m-PD molecule forms bonds with two epoxy groups of the SU8 monomer, leading to a tertiary amine configuration. This is in line with the well-established behavior of amines reacting with epoxy groups. Furthermore, the calculated band gap for this configuration, 4.4 eV, which does not fall within the range of the observed green light emission in our absorption and emission spectra. Figure 5 (b) presents an alternative configuration where one m-PD molecule bridges two SU8 monomers by forming two amide bonds. The calculated band gap for this structure is 3.6 eV, which aligns with the energy range corresponding to green fluorescence. This configuration supports the FTIR spectra, where a new peak at 1080 cm^{-1} , indicative of C-N stretching vibrations associated with amide bonds, is evident. Figure 5 (c) shows another possible configuration, this time featuring the formation of nitro (N-O) groups. In this scenario, one amine group from the m-PD molecule forms an amide bond with the SU8 monomer, while the other amine group creates an N-O bond. The band gap for this structure is calculated to be 3.6 eV, which fits well within the energy requirements for green light emission. Yet, this structure is not fully supported by FTIR. Lastly, Figure 5 (d) proposes a complex scenario involving m-PD dimerization via N-N bond formation. The resulting dimer interacts with SU8 epoxy groups, leading to the formation of amide bonds. Despite the theoretically calculated band gap of 2.6 eV being compatible with green fluorescence, the FTIR spectra do not provide explicit indications of N-N bond formation, suggesting this configuration may not substantially contribute to the overall characteristics of the m-PD-SU8 composite.

Our DFT calculations and corresponding experimental data suggest that tertiary amine formation involving two epoxy groups is the most probable outcome of the m-PD-SU8 interaction, as shown in Figure 3 (e). Other plausible configurations, such as those involving secondary amines, amide bonds, and potentially N-N and N-O bonds, may also exist but likely contribute less significantly to the overall properties of the synthesized material. For a more comprehensive analysis of possible molecular structures (Figure S4 and discussion).



ARTICLE

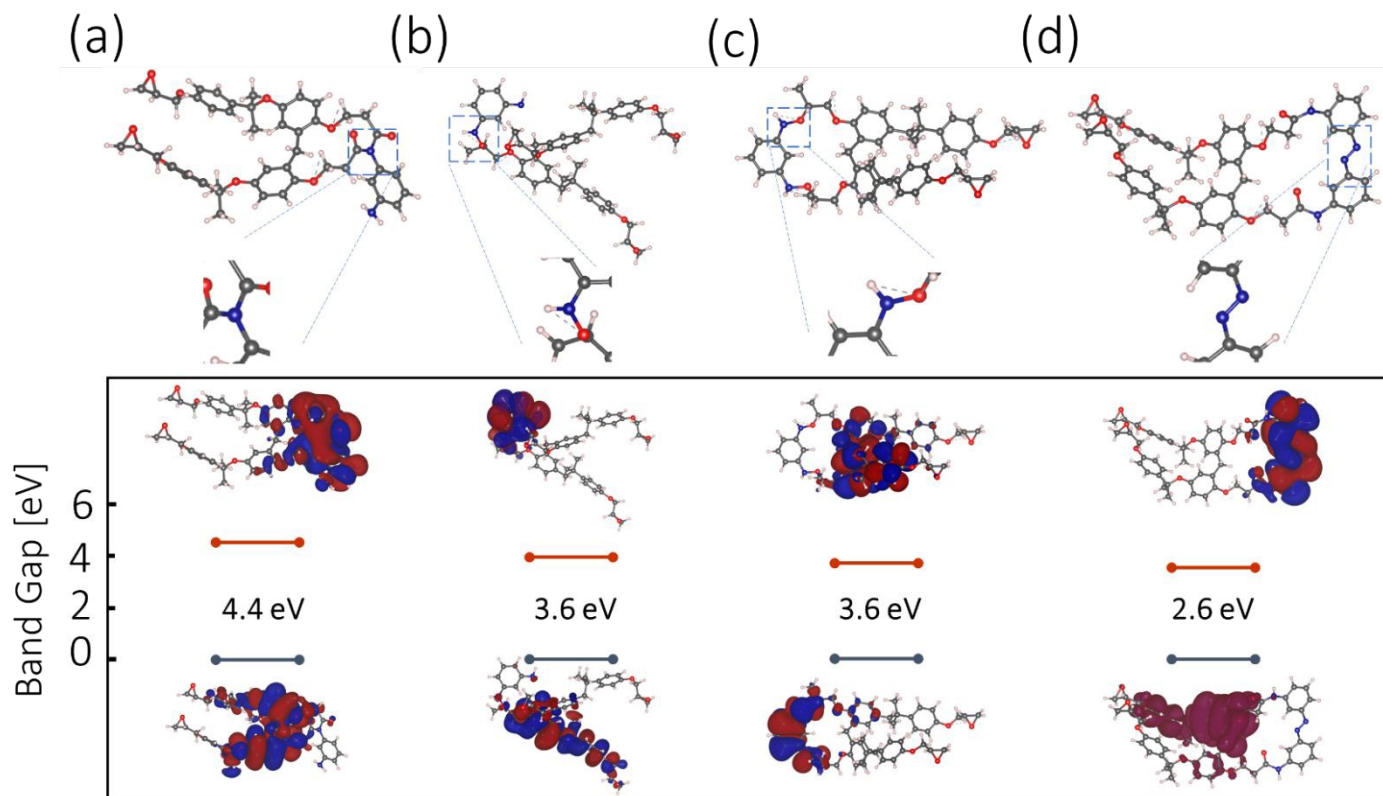


Figure 5: (a-d) Probable molecular structures of the m-PD-SU8 composite. The structures visualize the possible conformations resulting from the interaction between m-PD molecules and SU8 polymers. Each structure is represented as (a) (b) (c) and (d), demonstrating different plausible formations with band gap energies suitable for green emission. These structures were visualized and rendered using the VESTA software. Alongside each molecular structure, the calculated band gaps are provided, accompanied by the respective highest occupied molecular orbital (HOMO, shown at the bottom) and lowest unoccupied molecular orbital (LUMO, shown at the top) charge distributions.

Thin Films deposition and Surface Functionalization

Owing to the well-established adhesive properties of SU8 on a wide range of surfaces, it is crucial to evaluate the performance of our newly developed fluorescent derivative when forming thin film deposition on BK7 glass and indium tin oxide (ITO) coated glass. These substrates were chosen due to their common usage in optical and electronic applications, respectively. To explore the adhesion and film formation of SU8-m-PD, we prepared thin films of each material using the spin coating method. Consistent parameters were maintained to ensure comparability. The spin-coating process was conducted at speeds of 2k, 3k, and 4k RPM. Importantly, we found that the film thickness is identical to what appears in the SU8 2000.5 datasheet.



ARTICLE

The cross-sections of the SU8-m-PD conjugate thin films deposited on glass substrates are depicted in the HRSEM images in Figure 6. Specifically, Figure 6 (b) showcases a cross-section captured in backscatter mode, revealing a consistent thickness of about 300 nm. Figure 6 (a), captured in normal mode, illustrates the uniformity of the film structure, with its inset providing a closer look at a specific area at higher magnification. These images attest to the effectiveness of the spin-coating process executed at 6000 RPM.

Figure 6 (c) shows an AFM (Atomic Force Microscopy) topographical depiction of a compact 5x5 μm area of the SU8-m-PD thin film. The image effectively demonstrates the film's minimal surface roughness and superb uniformity, both critical attributes for enhancing device performance. The confocal microscopy images presented in Figure 6 (d) offer a comprehensive perspective on the fluorescence profiles of the SU8-m-PD conjugate films in three Cartesian planes (XY, XZ, YZ). The uniform distribution of fluorescence throughout the film shows the effectiveness of the m-PD conjugation process, which has potentially broad applications in bioimaging. For instance, the film could serve as a contrast agent in fluorescence microscopy or as a biomarker in cellular imaging, offering enhanced visualization of biological samples.

In the Supplementary Materials, Figure S4 provides a deeper insight into the surface features of the m-PD-SU8 thin film. The Atomic Force Microscopy (AFM) topographical images clearly illustrate the film's exceptional surface uniformity and near-negligible roughness. This uniformity and smoothness are crucial properties, especially considering the intended optoelectronic applications where surface irregularities could compromise the performance of the devices. Figure S6 illustrates the potential of our synthesized m-PD-SU8 composite. In part (a), a Scanning Electron Microscopy (SEM) image that shows the composite's conformality as it impeccably coats a capillary fiber, attesting to its potential in applications demanding intricate conformal coatings such as in optoelectronics and bio-compatible devices. Figure S6 (b) shows an optical fluorescence image that reveals the capillary with green SU8 emission under UV excitation, highlighting the composite's promising prospects in fluorescence-based applications, including optical sensors and imaging systems. The demonstrated integration of the m-PD-SU8 composite into a fiber optic context thus underscores its promise in advanced photonic devices.



ARTICLE

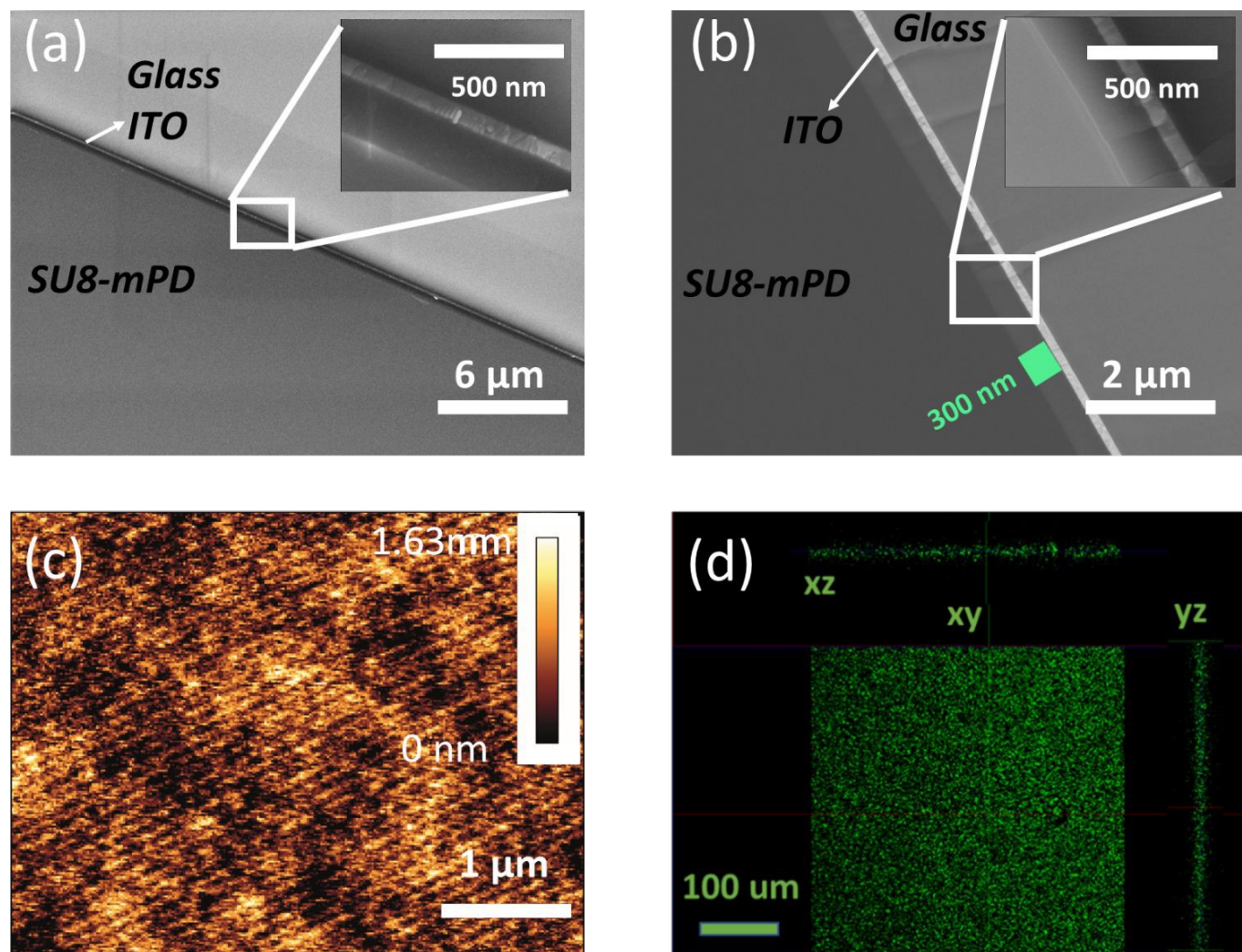


Figure 6: Characterization of the SU8-m-PD conjugated thin films. **(a)** HRSEM image of the m-PD conjugated film in normal mode, showcasing the adherence and consistency of the film with an inset displaying an enlarged view of a marked area at higher magnification. **(b)** HRSEM image of a cross-section of the m-PD conjugated film on a substrate, captured in backscatter mode, illustrating the film's thickness and uniformity, with an inset providing a magnified perspective of a designated region. **(c)** High-resolution AFM image of a $5 \times 5 \mu\text{m}$ area of the m-PD-SU8 film, demonstrating minimal surface roughness and high uniformity. **(d)** Confocal images in XY, XZ, and YZ planes of the m-PD film deposited on a glass substrate under 488 nm excitation, presenting the film's fluorescence profiles and spatial distribution.



ARTICLE

Conclusions

In our detailed study, we employed a series of analytical techniques to understand the synthesis and properties of SU8 polymers conjugated with phenylenediamine isomers, emphasizing meta-phenylenediamine (m-PD). Optical spectroscopy highlighted distinct optical behaviors of the conjugated polymers, with well-defined excitation and emission peaks. The FTIR spectra confirmed the presence of molecular bonding associated with conjugation, complemented by shifts in the ^1H NMR data, which indicated molecular modifications in the synthesized material. XPS analyses further showcased specific chemical functionalities in line with the proposed synthetic route. Furthermore, the estimated value of m-PD conjugates per SU8 monomers based on XPS elemental analysis was performed, suggesting more insights into the polymer functionality and ability for microlithography. While the results are promising, we remain conscious that the models presented are interpretations based on current data. Factors such as HCl concentration and polymer viscosity were methodically examined, and their influences on the optical properties of the conjugates were elucidated. ESEM and confocal microscopy visuals provided additional insights into the uniformity and consistency of the deposited materials on varied substrates, from flat films to contoured capillaries.

The approach of epoxy-amine conjugation, as outlined, suggests its potential in pioneering the development of polymers with unique optical and mechanical properties. Guided by these findings, this study hopes to contribute constructively to further research in surface-functionalized polymers and their potential applications.

Author Contributions

Hani Barhum: Investigation, Formal analysis, Methodology, Writing - original draft, Writing - review & editing. **Dennis Kolchanov:** Investigation, Formal analysis. **Mohammad Attrash:** Investigation, Formal analysis, DFT **Razan Unis:** Investigation, Formal analysis. **Janis Alnis:** Investigation, Formal analysis. **Toms Salgals:** Investigation, Formal analysis. **Ibrahim Yehia:** Investigation, Formal analysis. **Pavel Ginzburg:** Conceptualization, Writing - review & editing, Supervision.

Conflicts of interest

There are no conflicts to declare.

Acknowledgements



ARTICLE

This research was funded by the ERC StG "In Motion" (802279), PAZY Foundation (Grant No. 01021248), Tel Aviv University Breakthrough Innovative Research Grant, the Ministry of Science, Technology and Space of Israel (Grant No. 79518). Also, European Regional Development Fund project 1.1.1.5/19/A/003. We wish to thank Professor Joan Adler for the access to computational resources in the facility.

Notes and references

- (1) LaBianca, N. C.; Gelorme, J. D. <title>High-Aspect-Ratio Resist for Thick-Film Applications</Title>. In *Advances in Resist Technology and Processing XII*; 1995; Vol. 2438. <https://doi.org/10.1117/12.210413>.
- (2) Shaw, J. M.; Gelorme, J. D.; LaBianca, N. C.; Conley, W. E.; Holmes, S. J. Negative Photoresists for Optical Lithography. *IBM J Res Dev* **1997**, *41* (1–2). <https://doi.org/10.1147/rd.411.0081>.
- (3) Feng, R.; Farris, R. J. Influence of Processing Conditions on the Thermal and Mechanical Properties of SU8 Negative Photoresist Coatings. *Journal of Micromechanics and Microengineering* **2003**, *13* (1). <https://doi.org/10.1088/0960-1317/13/1/312>.
- (4) Lin, C. H.; Lee, G. Bin; Chang, B. W.; Chang, G. L. A New Fabrication Process for Ultra-Thick Microfluidic Microstructures Utilizing SU-8 Photoresist. *Journal of Micromechanics and Microengineering* **2002**, *12* (5). <https://doi.org/10.1088/0960-1317/12/5/312>.
- (5) Hamdi, F. S.; Woytasik, M.; Couty, M.; Francais, O.; Le Pioufle, B.; Dufour-Gergam, E. Low Temperature Irreversible Poly(DiMethyl) Siloxane Packaging of Silanized SU8 Microchannels: Characterization and Lab-on-Chip Application. *Journal of Microelectromechanical Systems* **2014**, *23* (5). <https://doi.org/10.1109/JMEMS.2014.2331454>.
- (6) Talebi, M.; Woias, P.; Cobry, K. Analysis of Impedance Data from Bubble Flow in a Glass/SU8 Microfluidic Device with on-Channel Sensors. *Sens Actuators A Phys* **2018**, *279*. <https://doi.org/10.1016/j.sna.2018.07.004>.
- (7) Talebi, M.; Cobry, K.; Sengupta, A.; Woias, P. Transparent Glass/SU8-Based Microfluidic Device with on-Channel Electrical Sensors; 2017. <https://doi.org/10.3390/proceedings1040336>.
- (8) Krishna, B.; Chaturvedi, A.; Mishra, N.; Das, K. Nanomechanical Characterization of SU8/ZnO Nanocomposite Films for Applications in Energy-Harvesting Microsystems. *Journal of Micromechanics and Microengineering* **2018**, *28* (11). <https://doi.org/10.1088/1361-6439/aae10c>.
- (9) Ransley, J. H. T.; Watari, M.; Sukumaran, D.; McKendry, R. A.; Seshia, A. A. SU8 Bio-Chemical Sensor Microarrays. *Microelectron Eng* **2006**, *83* (4–9 SPEC. ISS.). <https://doi.org/10.1016/j.mee.2006.01.175>.
- (10) Bêche, B.; Gaviot, E.; Godet, C.; Zebda, A.; Potel, A.; Barbe, J.; Camberlein, L.; Vié, V.; Panizza, P.; Loas, G.; Hamel, C.; Zyss, J.; Huby, N. Spin Coating and Plasma Process for 2.5D and Hybrid 3D Micro-Resonators on Multilayer Polymers. In *Optical Sensors 2009*; 2009; Vol. 7356. <https://doi.org/10.1117/12.820339>.



ARTICLE

- (11) Bêche, B. Integrated Photonics Devices on SU8 Organic Materials. *International Journal of Physical Sciences*. 2010.
- (12) Müller, R.; Cristea, D.; Kusko, M.; Obreja, P.; Esinenco, D.; Damian, V.; Logofatu, P. C. SU8 Polymer Materials Used in Integrated Optic Microsystems. *Optoelectronics and Advanced Materials, Rapid Communications* **2010**, *4* (2).
- (13) Gorissen, B.; Van Hoof, C.; Reynaerts, D.; De Volder, M. SU8 Etch Mask for Patterning PDMS and Its Application to Flexible Fluidic Microactuators. *Microsyst Nanoeng* **2016**, *2*.
<https://doi.org/10.1038/micronano.2016.45>.
- (14) Yardi, S.; Gupta, A.; Sundriyal, P.; Bhatt, G.; Kant, R.; Boolchandani, D.; Bhattacharya, S. High Efficiency Coupling of Optical Fibres with SU8 Micro-Droplet Using Laser Welding Process. *Lasers in Manufacturing and Materials Processing* **2016**, *3* (3). <https://doi.org/10.1007/s40516-016-0027-6>.
- (15) Tian, Y.; Shang, X.; Wang, Y.; Lancaster, M. J. Investigation of SU8 as a Structural Material for Fabricating Passive Millimeter-Wave and Terahertz Components. *Journal of Micro/Nanolithography, MEMS, and MOEMS* **2015**, *14* (4). <https://doi.org/10.1117/1.jmm.14.4.044507>.
- (16) Matarèse, B. F. E.; Feyen, P. L. C.; Falco, A.; Benfenati, F.; Lugli, P.; Demello, J. C. Use of SU8 as a Stable and Biocompatible Adhesion Layer for Gold Bioelectrodes. *Sci Rep* **2018**, *8* (1).
<https://doi.org/10.1038/s41598-018-21755-6>.
- (17) Wan, J.; Deng, S. R.; Yang, R.; Shu, Z.; Lu, B. R.; Xie, S. Q.; Chen, Y.; Huq, E.; Liu, R.; Qu, X. P. Silicon Nanowire Sensor for Gas Detection Fabricated by Nanoimprint on SU8/SiO₂/PMMA Trilayer. *Microelectron Eng* **2009**, *86* (4–6). <https://doi.org/10.1016/j.mee.2008.12.022>.
- (18) Charlot, S.; Gué, A. M.; Tasselli, J.; Marty, A.; Abgrall, P.; Estève, D. A Low Cost and Hybrid Technology for Integrating Silicon Sensors or Actuators in Polymer Microfluidic Systems. *Journal of Micromechanics and Microengineering* **2008**, *18* (1). <https://doi.org/10.1088/0960-1317/18/1/017003>.
- (19) Lorenz, H.; Despont, M.; Fahrni, N.; LaBianca, N.; Renaud, P.; Vettiger, P. SU-8: A Low-Cost Negative Resist for MEMS. *Journal of Micromechanics and Microengineering* **1997**, *7* (3).
<https://doi.org/10.1088/0960-1317/7/3/010>.
- (20) McNie, M.; King, D.; Vizard, C.; Holmes, A.; Lee, K. W. High Aspect Ratio Micromachining (HARM) Technologies for Microinertial Devices. *Microsystem Technologies* **2000**, *6* (5).
<https://doi.org/10.1007/s005420000044>.
- (21) Rajendran, J.; Sathiamoorthy, S.; Tiwari, K. J.; Suraj, T. S.; Ramachandra Rao, M. S.; Malar, P. Growth of Antimony Selenide Solar Absorber on Micro Textured Substrates for Efficient Light Trapping and Enhanced Optical Absorption. *Solar Energy* **2020**, *211*.
<https://doi.org/10.1016/j.solener.2020.10.030>.
- (22) Ramirez, J. C.; Schianti, J. N.; Almeida, M. G.; Pavani, A.; Panepucci, R. R.; Hernandez-Figueroa, H. E.; Gabrielli, L. H. Low-Loss Modified SU-8 Waveguides by Direct Laser Writing at 405 Nm. *Opt Mater Express* **2017**, *7* (7). <https://doi.org/10.1364/ome.7.002651>.
- (23) Maimon, R.; Perlson, E. Muscle Secretion of Toxic Factors, Regulated by MiR126-5p, Facilitates Motor Neuron Degeneration in Amyotrophic Lateral Sclerosis. *Neural Regeneration Research*. 2019.
<https://doi.org/10.4103/1673-5374.250571>.



ARTICLE

- (24) Kamande, J. W.; Wang, Y.; Taylor, A. M. Cloning SU8 Silicon Masters Using Epoxy Resins to Increase Feature Replicability and Production for Cell Culture Devices. *Biomicrofluidics* **2015**, *9* (3). <https://doi.org/10.1063/1.4922962>.
- (25) Choi, S. H.; Kim, Y. H.; Hebisch, M.; Sliwinski, C.; Lee, S.; D'Avanzo, C.; Chen, H.; Hooli, B.; Asselin, C.; Muffat, J.; Klee, J. B.; Zhang, C.; Wainger, B. J.; Peitz, M.; Kovacs, D. M.; Woolf, C. J.; Wagner, S. L.; Tanzi, R. E.; Kim, D. Y. A Three-Dimensional Human Neural Cell Culture Model of Alzheimer's Disease. *Nature* **2014**, *515* (7526). <https://doi.org/10.1038/nature13800>.
- (26) Altman, T.; Ionescu, A.; Ibraheem, A.; Priesmann, D.; Gradus-Pery, T.; Farberov, L.; Alexandra, G.; Shelestovich, N.; Dafinca, R.; Shomron, N.; Rage, F.; Talbot, K.; Ward, M. E.; Dori, A.; Krüger, M.; Perlson, E. Axonal TDP-43 Condensates Drive Neuromuscular Junction Disruption through Inhibition of Local Synthesis of Nuclear Encoded Mitochondrial Proteins. *Nat Commun* **2021**, *12* (1). <https://doi.org/10.1038/s41467-021-27221-8>.
- (27) Pelletier, N.; Bêche, B.; Tahani, N.; Zyss, J.; Camberlein, L.; Gaviot, E. SU-8 Waveguiding Interferometric Micro-Sensor for Gage Pressure Measurement. *Sens Actuators A Phys* **2007**, *135* (1). <https://doi.org/10.1016/j.sna.2006.07.012>.
- (28) Pelletier, N.; Bêche, B.; Gaviot, E.; Camberlein, L.; Grossard, N.; Polet, F.; Zyss, J. Single-Mode Rib Optical Waveguides on SOG/SU-8 Polymer and Integrated Mach-Zehnder for Designing Thermal Sensors. *IEEE Sens J* **2006**, *6* (3). <https://doi.org/10.1109/JSEN.2006.874489>.
- (29) Zebda, A.; Camberlein, L.; Bêche, B.; Gaviot, E.; Bêche, E.; Duval, D.; Zyss, J.; Jézéquel, G.; Solal, F.; Godet, C. Spin Coating and Plasma Process for 2.5D Integrated Photonics on Multilayer Polymers. *Thin Solid Films* **2008**, *516* (23). <https://doi.org/10.1016/j.tsf.2008.04.095>.
- (30) Falco, A.; Matarese, B.; Feyen, P.; Benfenati, F.; Lugli, P.; De Mello, J. C. Investigation of the Stability and Biocompatibility of Commonly Used Electrode Materials in Organic Neurooptoelectronics. *IEEE Trans Nanotechnol* **2016**, *15* (5). <https://doi.org/10.1109/TNANO.2016.2536946>.
- (31) LI, J.; ZHAO, Y.; GE, M.; FU, S.; LIN, T. Superhydrophobic and Luminescent Cotton Fabrics Prepared by Dip-Coating of APTMS Modified SrAl₂O₄:Eu²⁺, Dy³⁺ Particles in the Presence of SU8 and Fluorinated Alkyl Silane. *Journal of Rare Earths* **2016**, *34* (7). [https://doi.org/10.1016/S1002-0721\(16\)60075-3](https://doi.org/10.1016/S1002-0721(16)60075-3).
- (32) Apter, B.; Lapshina, N.; Barhom, H.; Fainberg, B.; Handelman, A.; Accardo, A.; Diaferia, C.; Ginzburg, P.; Morelli, G.; Rosenman, G. Fluorescence Phenomena in Amyloid and Amyloidogenic Bionanostructures. *Crystals (Basel)* **2020**, *10* (8), 1–43. <https://doi.org/10.3390/cryst10080668>.
- (33) Bahrom, H.; Goncharenko, A. A.; Fatkhutdinova, L. I.; Peltek, O. O.; Muslimov, A. R.; Koval, O. Yu.; Eliseev, I. E.; Manchev, A.; Gorin, D.; Shishkin, I. I.; Noskov, R. E.; Timin, A. S.; Ginzburg, P.; Zyuzin, M. V. Controllable Synthesis of Calcium Carbonate with Different Geometry: Comprehensive Analysis of Particle Formation, Cellular Uptake, and Biocompatibility. *ACS Sustain Chem Eng* **2019**, *7* (23), 19142–19156. <https://doi.org/10.1021/acssuschemeng.9b05128>.
- (34) Lapshina, N.; Shishkin, I. I.; Nandi, R.; Noskov, R. E.; Barhom, H.; Joseph, S.; Apter, B.; Ellenbogen, T.; Natan, A.; Ginzburg, P.; Amdursky, N.; Rosenman, G. Bioinspired Amyloid Nanodots with Visible Fluorescence. *Adv Opt Mater* **2019**, *7* (5). <https://doi.org/10.1002/adom.201801400>.



ARTICLE

- (35) Barhum, H.; Alon, T.; Attrash, M.; Machnev, A.; Shishkin, I.; Ginzburg, P. Multicolor Phenylenediamine Carbon Dots for Metal-Ion Detection with Picomolar Sensitivity. *ACS Appl Nano Mater* **2021**. <https://doi.org/10.1021/ACSANM.1C02496>.
- (36) Vandevondele, J.; Krack, M.; Mohamed, F.; Parrinello, M.; Chassaing, T.; Hutter, J. Quickstep: Fast and Accurate Density Functional Calculations Using a Mixed Gaussian and Plane Waves Approach. *Comput Phys Commun* **2005**, *167* (2). <https://doi.org/10.1016/j.cpc.2004.12.014>.
- (37) Momma, K.; Izumi, F. VESTA 3 for Three-Dimensional Visualization of Crystal, Volumetric and Morphology Data. *J Appl Crystallogr* **2011**, *44* (6), 1272–1276. <https://doi.org/10.1107/S0021889811038970>.
- (38) Vandevondele, J.; Hutter, J. Gaussian Basis Sets for Accurate Calculations on Molecular Systems in Gas and Condensed Phases. *Journal of Chemical Physics* **2007**, *127* (11). <https://doi.org/10.1063/1.2770708>.
- (39) Miehlich, B.; Savin, A.; Stoll, H.; Preuss, H. Results Obtained with the Correlation Energy Density Functionals of Becke and Lee, Yang and Parr. *Chem Phys Lett* **1989**, *157* (3). [https://doi.org/10.1016/0009-2614\(89\)87234-3](https://doi.org/10.1016/0009-2614(89)87234-3).
- (40) Stephens, P. J.; Devlin, F. J.; Chabalowski, C. F.; Frisch, M. J. Ab Initio Calculation of Vibrational Absorption and Circular Dichroism Spectra Using Density Functional Force Fields. *Journal of Physical Chemistry®* **1994**, *98* (45), 11623–11627. <https://doi.org/10.1021/j100096a001>.
- (41) Machnev, A.; Ofer, D.; Shishkin, I.; Kozlov, V.; Diaferia, C.; Accardo, A.; Morelli, G.; Apter, B.; Inberg, A.; Rosenman, G.; Ginzburg, P. Amplified Spontaneous Emission and Gain in Highly Concentrated Rhodamine-Doped Peptide Derivative. *Scientific Reports* **2021**, *11*:1 **2021**, *11* (1), 1–10. <https://doi.org/10.1038/s41598-021-96982-5>.
- (42) Yamamoto, S.; Tanaka, K. Molecular Size Effect on Curing Process for Epoxy and Amine Mixture. *Nihon Reorogi Gakkaishi* **2021**, *49* (2). <https://doi.org/10.1678/rheology.49.55>.
- (43) Belhadj, O.; Hammiche, D.; Boukerrou, A.; Gérard, J. F.; Duchet, J. Effect of Alfa Fiber Loading on the Mechanical, Physical and Dielectric Properties of Epoxy-Amine Composite. *J Compos Mater* **2022**, *56* (23). <https://doi.org/10.1177/00219983221119269>.
- (44) Cuvellier, A.; Torre-Muruzabal, A.; Kizildag, N.; Daelemans, L.; Ba, Y.; De Clerck, K.; Rahier, H. Coaxial Electrospinning of Epoxy and Amine Monomers in a Pullulan Shell for Self-Healing Nanovascular Systems. *Polym Test* **2018**, *69*, 146–156. <https://doi.org/10.1016/j.polymertesting.2018.05.023>.
- (45) Morsch, S.; Wand, C. R.; Gibbon, S.; Irwin, M.; Siperstein, F.; Lyon, S. The Effect of Cross-Linker Structure on Interfacial Interactions, Polymer Dynamics and Network Composition in an Epoxy-Amine Resin. *Appl Surf Sci* **2023**, *609*. <https://doi.org/10.1016/j.apsusc.2022.155380>.
- (46) Puyadena, M.; Calafel, I.; González de San Román, E.; Martin, L.; González, A.; Irusta, L. Recyclable Epoxy Resin via Simultaneous Dual Permanent/Reversible Crosslinking Based on Diels–Alder Chemistry. *Macromol Chem Phys* **2021**, *222* (17). <https://doi.org/10.1002/macp.202100146>.
- (47) Pandita, S. D.; Wang, L.; Mahendran, R. S.; MacHavaram, V. R.; Irfan, M. S.; Harris, D.; Fernando, G. F. Simultaneous DSC-FTIR Spectroscopy: Comparison of Crosslinking Kinetics of an



ARTICLE

Epoxy/Amine Resin System. *Thermochim Acta* **2012**, *543*, 9–17.
<https://doi.org/10.1016/j.tca.2012.04.024>.

